International Journal of Biological Macromolecules 159 (2020) 1048–1061

Contents lists available at ScienceDirect

International Journal of Biological Macromolecules

journal homepage: http://www.elsevier.com/locate/ijbiomac

Cellulose nanocrystals from grape pomace and their use for the development of starch-based nanocomposite films

Caroline Corrêa de Souza Coelho [a,*], Raysa Brandão Soares Silva [b], Carlos Wanderlei Piler Carvalho [c], André Linhares Rossi [d], José António Teixeira [e], Otniel Freitas-Silva [c], Lourdes Maria Correa Cabral [c]

[a] PPGCAL/Instituto de Química, UFRJ, Cidade Universitária, Ilha do Fundão, 21949-900 Rio de Janeiro, RJ, Brazil
[b] Departamento de Engenharia Química e de Materiais, Pontifícia Universidade Católica do Rio de Janeiro, PUC-Rio, 38063, 2245-900, Rio de Janeiro, RJ, Brazil
[c] Embrapa Agroindústria de Alimentos, Av. das Américas 29501, 23020-470, Rio de Janeiro, RJ, Brazil
[d] Centro Brasileiro de Pesquisas Físicas, Rua Dr. Xavier Sigaud, 150 – Urca, Rio de Janeiro, RJ, Brazil
[e] Centre of Biological Engineering, Universidade do Minho, Campus de Gualtar, 4710-057, Braga, Portugal

ARTICLE INFO

Article history:
Received 30 January 2020
Received in revised form 25 April 2020
Accepted 6 May 2020
Available online 11 May 2020

Keywords:
Packaging
Biopolymers
Nanocomposites
Mechanical properties
Barrier properties

ABSTRACT

Nanocomposite films prepared from starch (ST) in the presence of cellulose nanocrystals (CNCs) was performed using grape pomace as raw material. CNCs were obtained by acid hydrolysis and added to filmogenic solutions (1, 2, 5, 10 and 15 g/100 g of ST). Cellulose, CNCs and Nanocomposites were characterized. Amorphous non-cellulosic materials were removed from the grape pomace presented values for CrI 64% and 71% and yield 12 and 70% in Cellulose and CNCs, respectively. Nanocomposites showed smaller permeability and the addition of 5 to 15% CNCs formed more opaque films and had improved tensile strength and Young's modulus. The addition of CNCs from 5 to 15% proved to be effective in improving mechanical properties and decreasing water vapor permeability, important characteristics in food packaging materials. This study provided an effective method to obtain CNCs from the agroindustrial waste and open the way to produce high-value starch based nanocomposites.
© 2020 Elsevier B.V. All rights reserved.

1. Introduction

Biodegradable packaging is usually obtained from biopolymers such as starch, chitosan and cellulose extracted from renewable resources such as agricultural waste or waste from food processing [1–3].

Starch (ST) is a polysaccharide widely available from different natural plant sources such as cereals, tubers and roots, also considered a promising biopolymer because it is biodegradable, renewable and of relatively low cost [3,4]. It is considered as a sustainable approach to the development of renewable biomaterials [5]. Amylose and amylopectin are the polymers that make up starch and are found in different proportions according to the raw material [6]. Amylopectin is responsible for starch's semicrystallinity and is a highly branched molecule composed of linear glucose chains linked by α (1–4) glycosidic bonds in the main chain and α (1–6) glycosidic bonds at branching points. The chains of this molecule are arranged perpendicularly on the surface of the granule along the main chain, so branch points are distributed to form amorphous and crystalline lamellae [7].

For starch to form cohesive films, degradation of the semicrystalline structure of the molecule must occur. Thus, shear, heat and forced from plasticizer addition are required so that the granules irreversibly lose the semicrystalline structure and are converted into a continuous matrix [8].

The use of starch-based packaging still faces obstacles because of its water vapor permeability and limited mechanical properties. Therefore, this biopolymer is usually added of other materials such nanoreinforcement, polymer blending, or chemical modification by crosslinking reaction to improve those characteristics [9]. As an example of this good compatibility with different biomaterials Koshy and co-authors used soy protein and starch-based to produce green composites [10] and Mohanty & Swain [11] used starch hybrid and graphene oxide, nano silver and sandwiched with poly(ethylmethacrylate) for packaging applications.

The reinforcement of ST films with cellulose nanocrystals (CNCs) may be a promising alternative to improve the mechanical performance and decrease the permeability of starch films, preserving the sustainable character of final composites [12,13]. Balakrishnan et al. [9] studied the effect of CNCs, isolated from pineapple leaf, on the starch composite and found that inclusion of CNC to thermoplastic starch improves the reinforcing property. Similarly, González et al. [14] observed higher stiffness due to increase of CNC content adding CNCs (2.5 and 5 wt%) isolated from microcrystalline cellulose as nanoreinforcement on the starch-

* Corresponding author.
E-mail addresses: carolcsc.agro@gmail.com (C.C.S. Coelho), raysabrandao@live.com (R.B.S. Silva), carlos.piler@embrapa.br (C.W.P. Carvalho), andrelinharesrossi@gmail.com (A.L. Rossi), jateixeira@deb.uminho.pt (J.A. Teixeira), otniel.freitas@embrapa.br (O. Freitas-Silva), lourdes.cabral@embrapa.br (L.M.C. Cabral).

https://doi.org/10.1016/j.ijbiomac.2020.05.046
0141-8130/© 2020 Elsevier B.V. All rights reserved.

based nanocomposite hydrogels. In another study Vaezi et al. [15] produced alpha cellulose of cotton linter, and found the bionanocomposites with 5 wt% NCC and montmorillonite showed the best improvements in its properties as highest disintegrability rate, good reduction in water vapor and oxygen permeability and mechanical properties.

Cellulose is a linear homopolysaccharide composed of β-D-glucopyranose units linked by β-1-4 bonds, is naturally available polymers with structure presents highly ordered crystalline domains and amorphous domains like pectin, lignin, hemicellulose etc. [16]. The reinforcing cellulose material in starch-based films appears particularly interesting due to the chemical similarities in the polysaccharide structure, which can lead to a good interfacial adhesion of the matrix-cellulose [17].

The amorphous domains of cellulose can be cleaved during the production processes of cellulose nanocrystals (CNCs) by selective hydrolysis using mechanical shear, chemical treatment, enzymatic hydrolysis action or by their combination [18]. Acid hydrolysis is a well-known strategy for CNC production [19–23] This treatment consists of longitudinal sectioning of the cellulose microfibrils; so that hydronium ions promote hydrolytic cleavage of glycosidic bonds in the amorphous domains, releasing individual crystallites. The resulting nanoparticles have dimensions and CrI that vary depending on the cellulose source and preparation procedure [22].

CNCs can be synthesized from lignocellulosic materials, algal cellulose, bacterial cellulose, microcrystalline cellulose and waste paper [12,24–28] and its geometric dimensions and shapes depend on the source of cellulose [29,30]. In the literature typical dimensions range from 4–25 nm in diameter and 100–1000 nm in length, however some authors refer to nanocrystals as needle-like cellulose particles with at least one dimension equal to or <100 nm [19,31–33]. Because CNCs are nanometric particles with the interesting properties, such as: biocompatible with natural polymers, biodegradable, non-toxic and also have high surface area and lightness, they have been evaluated as reinforcement material for a wide range of polymeric matrices, aiming to replace petrochemical-based products [34–36].

In a previous work [2] it was studied the production of the CNCs from the *Pinoir Noir* grape pomace and it could find the best process conditions for this production. In this work, besides to producing and characterizing CNCs from *Alicante Bouschet* grape pomace, it was compared their reinforcing efficiency and their action as a permeability moderators at different concentrations of CNCs in starch nanocomposite films.

2. Materials and methods

2.1. Materials

The pomace of the *Alicante Bouschet* grape variety, obtained from the red wine making process was used for the extraction of cellulose nanocrystals (CNCs). The sample from 2017 harvest was kindly provided by the Rio Sol winery (Lagoa Grande, Brazil). The material was transported frozen and stored at −18 °C until processed.

The grape pomace was dried at 60 °C for 18 h, in an oven with air circulation. The dried material was processed in a horizontal depulper Bonina 0.25 df (Itametal, Itabuna, Brazil), to separate the seeds from the pomace. The seeds were milled in a knife grinder A 11 (IKA Group, Staufen, Germany) and sieved for grain-size classification within the range from 0.177 mm to 0.425 mm (80 to 40 mesh Tyler). The milled pomace was packed in vacuum-sealed plastic bags, protected from light and kept at −5 °C until use.

2.2. Pomace pretreatment for cellulose production and cellulose nanocrystals

Cellulose was obtained by removing the non-cellulosic components from the pomace according to the procedure reported by Lu & Hsieh [37] and Coelho et al. [2] with some modifications.

The strategy consisted of four consecutive steps:

i) Treatment with ethanol solution (1:15 m_{pomace}:$v_{solution}$) at 75 °C for 3 h to remove wax, phenolics, pigments and oils,
ii) Treatment with 2% H_2SO_4 solution (1:20 $m_{pomace}/v_{solution}$) at 90 °C for 5 h to hydrolyze polysaccharides and acid-soluble polyphenols,
iii) Treatment with 5% NaOH solution (1:20 $m_{pomace}/v_{solution}$) at 90 °C for 5 h to dissolve the remaining hemicellulose, lignin and other polysaccharides,
iv) Bleaching (1:20 $m_{pomace}/v_{solution}$) with 5% H_2O_2 solution, pH 11.5 (adjusted with NaOH), at 50 °C for 8 h for two consecutive stages.

Between all steps, the solid material was washed with distilled water until reached pH 6–7 and then dried in air circulation oven SL 102/100 (Solab, Piracicaba, Brazil) at 40 °C and 10% RH. The resulting cellulosic pulp was frozen and lyophilized in a liophilyzer L101 (Liotop, São Carlos, Brazil).

CNCs were obtained by hydrolyzing cellulose with 64–65% m/m sulfuric acid at 45 °C, under constant stirring, in the proportion of 1 g cellulose:20 mL acid solution for 60 min, according to previous studies [2]. Hydrolysis was interrupted by dilution with ice. The recovered material was washed with distilled water to pH 4.0, and subjected to successive centrifugations (10,000 rpm, 20 min at 20 °C) until a colloidal suspension was formed. The supernatant was dialyzed using dialysis membranes (*Sigma-Aldrich*-D9402-100FT) against ultrapure water to neutral pH and homogenized with help of an ultrasound probe model 450 (Brason Ultrasonics Corp., Danbury, USA) set at 400 W, 20 Hz 40% of amplitude in cycles of 5 s *on* and 2 s *off*, totaling 10 min. The use of ice bath was necessary to avoid rise in temperature.

A diagram of the extraction cellulose process from grape pomace to produce CNCs is shown in Fig. 1.

CNCs were kept under refrigeration (7 °C) for stability studies and assessment of their morphologic structure by scanning-transmission electron microscopy (STEM) or lyophilized for thermogravimetric analysis (TGA) and X-ray diffraction (XRD). The initial dry mass used for acid hydrolysis and the final mass obtained after lyophilization were considered for yield calculation.

2.3. Film development

CNCs were used at five different levels: 1, 2, 5, 10 and 15% (w/w, dry basis) in order to prepare ST/CNCs nanocomposite film, described by Coelho et al. [1] and Li et al. [38] with some modifications. The filmogenic solution was prepared by mixing 2% g mL^{-1} of ST with water, under stirring, (400 rpm, 21 h at ±25 °C). Subsequently, the CNCs were added to this solution and stirred using an ultra-turrax disperser T18 (IKA Group, Staufen, Germany) at 600 rpm for 20 min. The amount of CNCs used was calculated from the concentration of the 5 g L^{-1} initial solution, and the water was added until working concentrations were achieved. The control sample did not contain CNCs. Glycerol, the plasticizer, was added at a fixed concentration of 25% based on the ST dry mass and left under stirring for 1 h.

To ensure complete dissolution of ST and the formation of a homogenous dispersion, the solutions were heated in a shaking water bath at 70 °C during 30 min under stirring (400 rpm). Temperature increasing was measured with a thermocouple placed at the geometric center of the sample volume. The resulting dispersion was sonicated for 20 min at 40 Hz in ultrasonic bath model 5510 (Brason Ultrasonics Corp., Danbury, USA), and vacuumed. The steps for filmogenic solution

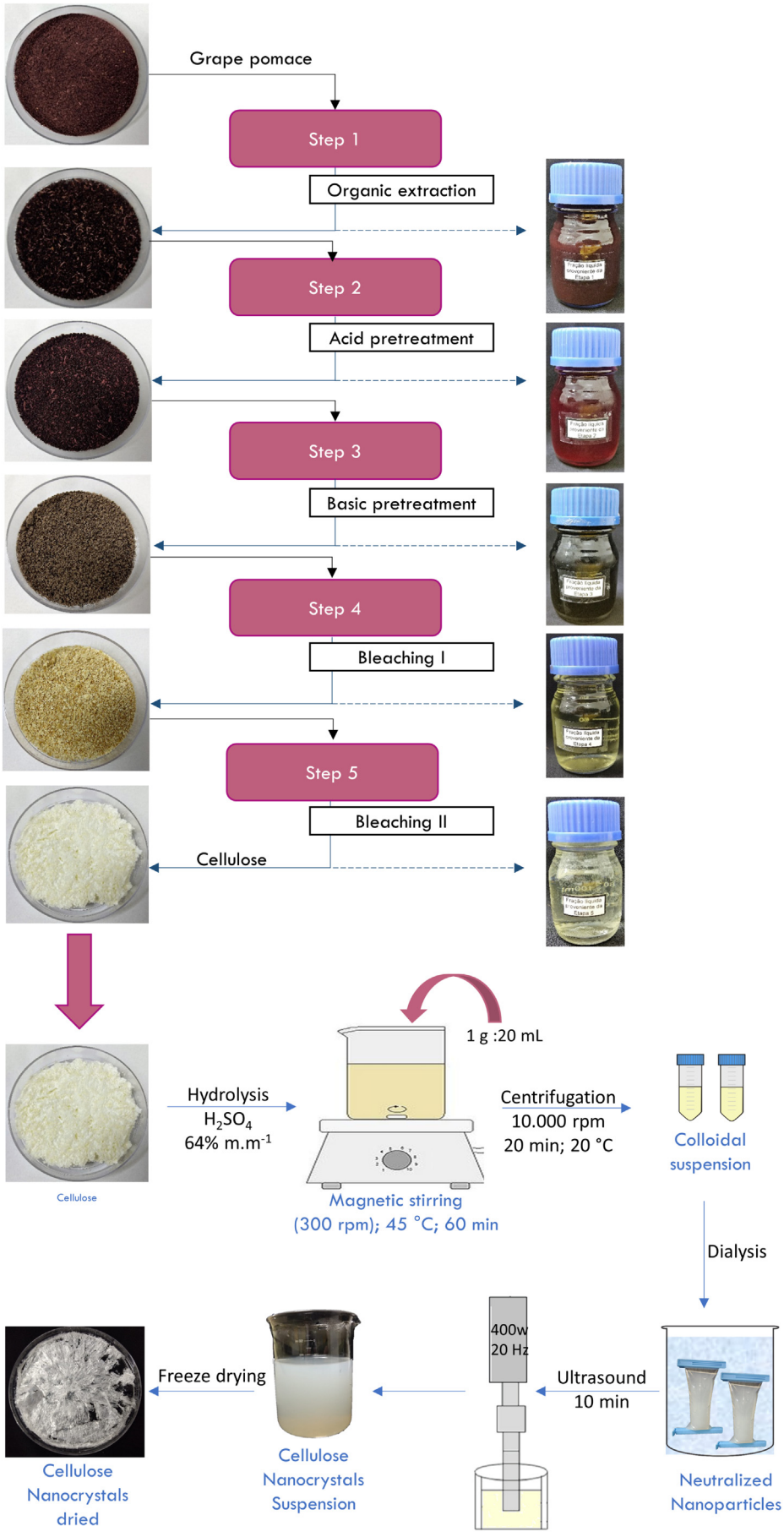

Fig. 1. Schematic representation of the pre-treatment steps of Alicante Bouschet grape pomace. Cellulose extraction, acid hydrolysis process and cellulose nanocrystal production.

development are represented in Fig. 2. The films were prepared using the casting technique, where a constant amount of filmogenic solution (28 mL) was casted in round acrylic plates (90 × 15 mm) and dried at 35 ± 1 °C for 24 h in oven with air circulation SL 102 (Solab, Piracicaba, Brazil).

2.4. Characterization of grape pomace, cellulose and cellulose nanocrystals

2.4.1. Yield analysis

The pretreatment yields were determined by the ratio between the final mass of the pomace in each step (dry basis) and the initial mass of the fresh (*in natura*) pomace (dry basis) according to Eq. (1):

$$\text{Yield}\ (\%) = (\text{Final mass}/\text{Initial mass}) \times 100 \quad (1)$$

2.4.2. Color analysis

The color of the samples was determined in a digital colorimeter model Chroma Meter CR-400 (Konica Minolta, Osaka, Japan), using the CIELab scale to determine L*, a* and b* color parameters [43]. The sample was poured in a Petri dish with 5 cm diameter covering the entire bottom of the dish, and the reading was performed in three different points. The total color difference (ΔE*) was calculated in relation to fresh pomace, according Eq. (2).

$$\Delta E* = \sqrt{(L^* - L_0{}^*)^2 + (a^* - a_0{}^*)^2 + (b - b_0{}^*)^2} \quad (2)$$

In this study, L^*_0, a^*_0 and b^*_0 stand for the values of the color parameters of fresh grape pomace and L^*, a^* and b^* for the values of the color parameters of the sample in each step.

2.4.3. Scanning electron microscopy (SEM)

The morphological aspect of the samples after each pretreatment step was evaluated in a thermionic TM3000 scanning electron microscope (Hitachi, Tokyo, Japan) with an acceleration voltage of 15 kV.

2.4.4. X-ray diffraction (XRD)

The X-ray diffraction patterns of grape pomace samples, cellulose and CNCs were analyzed between 2Θ = 5° and 2 Θ = 32° with a step of 0.04°.min^{-1} in an X-ray diffractometer (Bruker, Rheinfelden, Germany) working at 30 kV, 10 mA, a divergence slit width of 0.6 mm, a scatter slit width of 0.6 mm and a receiving slit width of 0.2 mm.

The crystallinity index (*CrI*) was determined according to Eq. (3).

$$CrI = \frac{I_{002} - I_{am}}{I_{002}} \times 100 \quad (3)$$

where I_{002} is the maximum intensity diffracted peak at $2\theta = 22.5°$, and *Iam* is the intensity attributed to the amorphous components at $2\theta = 18°$.

2.4.5. Scanning-transmission electron microscopy (STEM)

The samples were observed using a transmission electron microscope JEM-2100F (JEOL Ltd., Tokyo, Japan) operated at an acceleration voltage of 200 kV. The images were obtained in STEM mode using a dark field (DF) annular detector (JEOL). A 10 μL sample was deposited onto a TEM grid (ultrathin carbon film on Lacey Carbon Support film, 400 mesh, Copper, Ted Pella Inc., USA).

2.4.6. Thermogravimetric analysis (TGA)

Thermal stability was determined in a TGA-2000 automatic analyzer (Navas Instruments, South Carolina, USA). The samples (~0.5 g) were placed in the balance system and heated from 20 to 550 °C, at a heating rate of 20 °C min^{-1} under nitrogen atmosphere.

2.5. Film characterization

2.5.1. Packaging

Dried films were stored in desiccators at 25 °C and relative humidity of 54%, using a saturated solution of $Mg(NO_3)_2 6H_2O$.

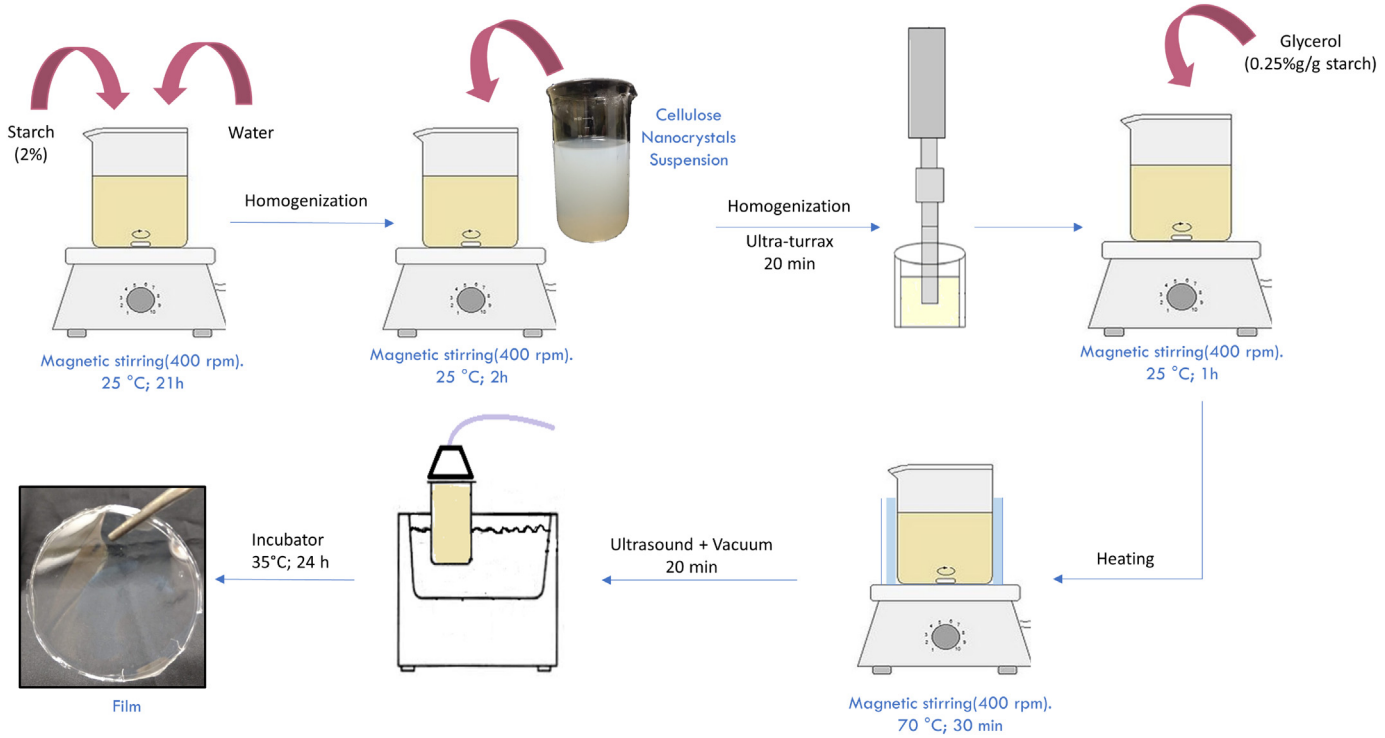

Fig. 2. Scheme for the production of starch films reinforced with cellulose nanocrystals (nanocomposites).

2.5.2. Thickness

Film thickness was measured with a portable micrometer (Starrett 232, São Paulo, Brazil). Thickness measurements were taken at ten randomic points and the mean value was used to determine water vapor permeability and mechanical properties.

2.5.3. Moisture content (MC)

Films were dried at 105 °C in an air-circulating oven for 24 h. The mass of the films before and after drying was determined gravimetrically and moisture content was calculated using Eq. (4):

$$MC(\%) = \frac{Mi - Mf}{Mi}.100 \quad (4)$$

where Mi and Mf are the masses of the initial and dried samples, respectively. The experiments were performed in triplicate and expressed the percentage of water removed from the initial sample.

2.5.4. Film solubility (Sol)

Film solubility (Sol) in water was determined by immersion of the dry films in water as reported by Cuq, Gontard, Cuq, & Guilbert [39]. Solubility value was calculated using Eq. (5)

$$Sol\ (\%) = \frac{Mi\prime - Mf\prime}{Mi\prime}.100 \quad (5)$$

where Mi is the initial mass of the sample, Mf the final mass of the sample and Sol represents the solubility percentage of the film.

Triplicates of each film were cut into circles of 2 cm diameter, dried at 105 °C in oven for 24 h and weighed. Then, the samples were immersed into 50 mL of water, sealed with paraffin and shaken in an orbital shaker at 60 rpm for 24 h at 25 °C. The non-soluble portion of each film was removed and dried at 105 °C in an oven during 24 h and weighed again to determine the weight of the dry matter.

2.5.5. Water vapor permeability (WVP)

WVP of the films was gravimetrically determined based on ASTM E96–92 method [40]. The film was sealed on the top of a permeation cell containing distilled water (100% RH; vapor pressure of 2337 Pa at 25 °C) and placed in a desiccator with silica gel at 25 °C and 0% RH (0 Pa water vapor pressure). The cups were weighed at 2 h intervals during 8 h. The water transferred through the film and adsorbed by the desiccant was determined from the weight loss of the permeation cell.

Steady and uniform state of water pressure conditions were assumed by keeping constant air circulation outside the test cup by means of a miniature fan placed inside the desiccators [41]. The slope of the curve representing weight loss versus time was obtained by linear regression.

2.5.6. Contact angle

An optical contact angle meter *CAM 101* (KSV Instruments Ltd., Helsinki, Finland) was used to measure the contact angle on the film surface by sessile drop method [42]. Each measurement was taken within 10 s with a 500 μL syringe (Hamilton, Reno, USA) and 0.75 mm diameter needle. At least 10 measurements were taken for each sample at ±25 °C.

2.5.7. Apparent color and opacity

The color of the films was determined with a spectrophotometer Chroma Meter CM-5 (Konica Minolta, Tokyo, Japan). The CIELab scale was used to determine the color parameters L*, a* and b * [43]. Opacity (Y) was determined from the relationship between the opacity of each sample on the black standard (Yb) and the opacity of the sample on the white standard (Yw) [44], using Eq. (6).

$$Y\ (\%) = \frac{Yb}{Yw}.100 \quad (6)$$

where Yb and Yw are the opacities on the black and white patterns, respectively. The samples were analyzed in triplicate.

2.5.8. Scanning electron microscopy (SEM)

The effect of CNC incorporation in the film was obtained in relation to surface and cross-section morphology using a scanning electron microscope (SEM) TM3000 (Hitachi, Tokyo, Japan) with acceleration voltage of 15 kV under vacuum condition.

2.5.9. Mechanical properties

The films were analyzed as their performance in the tensile test in a Texture Analyzer TA XT Plus (Stable Microsystems, Surrey, UK), fit with a load cell of 30 kg, following the ASTM D 882-02 (2010) method. The films were sized on 120 mm long and 20 mm wide specimens. These specimens were fixed in the equipment grips with initial distance between them of 100 mm and tensile speed of 5 mm min^{-1}. The stress at break was determined by the relation between load and the initial cross-sectional area of the film. Strain at break was determined by the stress-strain curve (linear strain [(l - lo)/lo]). Young's modulus or modulus of elasticity was determined in the linear region. Results were analyzed using Texture Exponent 32, version 6.0 software (Stable Microsystems, Surrey, UK).

2.5.10. X-ray diffraction (XRD)

X-ray diffraction patterns of the samples were analyzed between $2\Theta = 4$ and $2\Theta = 30$ with a step of $2\Theta = 0.02°$ in a bench X-ray diffraction instrument D2 Phaser (Bruker, Rheinfelden, Germany) working at 30 kV, 10 mA, a divergence slit width of 0.6 mm, a scatter slit width of 0.6 mm and a receiving slit width of 0.2 mm.

2.5.11. Thermogravimetric analysis (TGA)

Thermogravimetric analysis (TGA) was conducted in an automatic analyzer TGA-2000 (Navas Instruments, South Carolina, USA). The samples (~0.5 g) were heated from 20 to 450 °C at a heating rate of 10 °C min^{-1}, under nitrogen atmosphere (with flow speed of 30 mL. min^{-1}). The thermogravimetric curves (TG) show the mass loss of the samples analyzed as a function of heating temperature, while the curves of the first derivative (DTG) show the speed of the sample's mass loss as a function of temperature. They are used to identify the temperature peaks where thermal degradation of the sample occurs. Analyses were carried out in triplicate.

2.6. Statistical analysis

One-way ANOVA was applied for data analysis, when observed significant differences between treatments, the means were compared according to Tukey's test at significance level of 5% (= 0.05). Statistical analyses were performed using the Statistica version 8.0 (StatSoft Inc., Tulsa, USA).

3. Results and discussion

3.1. Characterization of pretreatment of grape pomace residue and cellulose nanocrystals

3.1.1. Yield analysis

The pretreatment process applied to fresh grape pomace to obtain cellulose presented a yield of about 12%. The extraction yield was lower than that reported by Lu & Hsieh [37], who obtained an extraction yield of 16.4% for cellulose from grape skin using a similar extraction protocol. Coelho et al. [2] extracted up to 10% cellulose from grape pomace, using an extraction method very similar to that used in this study. These results show the influence of the type of residue and the extraction process used. The use of hydrolysis can potentiate CNC yield from grape pomace by up to 70% ± 7.06 [2]. Acid concentration, reaction time, amount of cellulose per volume of acid used, cellulose purity and

methods applied for nanocellulose separation are factors that can influence on CNC production [45,46].

3.1.2. Color analysis

The effect of different chemical treatments on the visual appearance of the raw material during cellulose isolation can be observed in Fig. 1. The Table 1 shows the color values for each process step.

The fresh sample showed color characteristic of red grape skin, being close to the middle of the chromacity diagram a*, b* and dark hue (L*). Demirkol and Tarakci [47] analyzed grape pomace (cv Isabella), dried in oven at 60 °C and observed a* (red component) values and b* (yellow component) values similar to this study (17.33 and 5.10, respectively), however the pomaces were darker (22.86, L*), which may be due to the differences in the cultivars studied.

After ethanol treatment it was possible to observe a slight trend from red to yellow, because °hue presented values around 20.01°. In relation to Chroma, low values represent less vivid color intensity; L* and a* values were lower, characterizing a darker and less reddish-purple sample when compared to the fresh sample ($p < .05$). More accentuated darkening was observed after acid treatment, although Chroma presented a higher value than that of previous step ($p < .05$), the value found represents not very vivid color intensity, with °hue similar to the previous step. In the alkaline treatment, constituents such as starch, pectin and hemicellulose are hydrolyzed [48] making the sample more yellowish, 50.77° ($p < .05$), due to °hue and became lighter (L* 40.48; $p < .05$).

Bleaching I promoted lighter brown color, despite the good lightness gain (37.51 in the fresh waste and 76.69 in this step), the yellowish color of the residue with °hue of 80.85° and b* of 20.62, indicates the presence of residual lignin impregnating the fibers [49]. On the other hand, after bleaching II there was a gradual discoloration from brown to white, with higher values of L*and °hue ($p < .05$), with a more significant color difference compared to the fresh sample (ΔE 75 ± 0.40; $p < .05$), indicating successful removal of the remaining lignin responsible for the yellowish color [48]. Consequently, the purification process eliminated initial non-cellulosic components and the impurities of the final product.

The H_2O_2, used as bleaching agent, resulted in the generation of highly reactive species of superoxide radicals (O_2-), responsible for the oxidation of lignin aromatic rings and parts of hemicellulose by carboxylic acids. In this sense, bleaching removed the chromophore groups from the raw material fiber [50]. Lu & Hsieh [37] and Jiang and Hsieh [20] evidenced the effectiveness of alkaline H_2O_2 during the bleaching stage in grape and tomato skins.

3.1.3. Morphology of grape pomace and cellulose nanocrystals

The fresh sample (*in natura)* (Fig. 3A) showed fiber bundles and an irregular surface consisting of lignin, hemicelluloses and other extractives such as waxes and pectins that may be adhered to the raw material.

After ethanol (Fig. 3B), sulfuric acid (Fig. 3C) and alkaline (Fig. 3D) treatments, the solid residue presented more separated fiber bundles which was mainly attributed to the removal of pectins, waxes, extractives, acid-soluble polysaccharides and polyphenols, hemicellulose and other polysaccharides soluble in alkaline medium [37].

After bleaching I (Fig. 3E), there was partial elimination of lignin from the fiber surface, which appears more exposed as evidenced by cracks. The cellulose extracted from pomace is shown in Fig. 3F. After bleaching II, the fiber surface became rougher and showed microfibril bundles, composed by fibrils, becoming more visible and slight detachable from the fibers, as described by Dufresne et al. [51], Lu & Hsieh [37] and Xie et al. [46].

The hydrolysis treatment with sulfuric acid and the ultrasound treatment were able to cleave transversally the amorphous region of cellulose microfibrils and CNCs were then obtained. In this manner, there was a reduction of fiber length from microns to nanometers [52,53]. STEM image of CNCs indicating regular needle shape is shown in Fig. 4. This morphology is similar to that of other CNCs obtained from other agroindustrial wastes [37,46,52,53].

3.1.4. X-ray diffraction (XRD)

XRD patterns of all studied samples are shown in Fig. 5. Both, cellulose from grape pomace and CNCs presented typical crystalline peaks of type I cellulose (2θ: 15–16° [110] and 22.5° [200]). The same crystalline structure was observed in CNCs obtained from different types of lignocellulosic wastes [23, 20,54,55].

More defined and high intensity peaks were observed in cellulose and CNC peaks. The cellulose presented *CrI* of 64% and CNCs 71% evidenced that the pretreatment steps were effective in removing a significant fraction of amorphous structures (hemicelluloses and lignin). Acid molecules diffuse more easily into cellulose amorphous regions, which are more susceptible to cleavage of glycoside bonds than the more compacted crystalline domains [23]. Coelho et al. [2] reported the efficiency of the production of cellulose and CNCs from Pinot Noir grape pomace and similar crystallinity indices. Crystallinity is an important factor for the use of this nanomaterial in nanocomposites, because it is responsible for much of the high stiffness provided by CNCs in polymeric matrices [22].

3.1.5. Thermal property analysis

The thermal degradation behavior of fresh grape pomace, cellulose and CNC was investigated by TGA and derivative thermogravimetric curve (DTG). The thermograms obtained are shown in Fig. 6.A and B and the correspondent data are listed in Table 2.

All samples showed a small mass decrease around 100 °C which results from the evaporation of adsorbed moisture, due to the hydrophilic nature of these cellulosic materials [2,23,52]. Fresh pomace and cellulose presented similar initial thermal degradation (T_{onset}), whereas CNCs showed the lowest T_{onset} and highest degradation temperature (T_{max}). The smaller thermal stability of CNCs when compared to the fresh pomace was also observed in CNCs from tomato skins [20], vine shoots [55] and pinneaple crown waste [23]. Such authors reported that sulfate groups, from the hydrolisis with H_2SO_4 on CNC surface,

Table 1
Pomace color parameters after bleaching and after different chemical pre-treatments conditions.

Solid waste	L*	a*	b*	*Chroma*	°Hue	ΔE
In natura (grape pomace)	37.51 ± 0.07^{d}	15.11 ± 0.05^{a}	4.45 ± 0.07^{c}	15.76 ± 0.03^{b}	16.58 ± 0.30^{d}	–
After ethanolic extraction	26.66 ± 0.05^{e}	12.25 ± 0.05^{c}	4.46 ± 0.09^{c}	13.04 ± 0.02^{d}	20.01 ± 0.45^{c}	42.99 ± 0.15^{c}
After acid extraction	24.25 ± 0.21^{f}	13.54 ± 0.07^{b}	5.13 ± 0.13^{c}	14.48 ± 0.11^{c}	20.74 ± 0.38^{c}	42.41 ± 0.29^{c}
After basic extraction	40.48 ± 0.43^{c}	6.52 ± 0.12^{d}	7.98 ± 0.09^{b}	10.31 ± 0.09^{e}	50.77 ± 0.68^{b}	42.90 ± 0.11^{c}
After bleaching I	76.69 ± 1.05^{b}	3.32 ± 0.07^{e}	20.62 ± 0.70^{a}	20.89 ± 0.68^{a}	80.85 ± 0.50^{b}	54.62 ± 1.00^{b}
After bleaching II (cellulose)	93.63 ± 0.59^{a}	-2.20 ± 0.10^{f}	7.39 ± 0.53^{b}	7.71 ± 0.53^{f}	106.61 ± 0.59^{a}	75.00 ± 0.40^{a}

Values in the same column followed by different letters are statistically different (Tukey test, $p < .05$).
Values reported are the mean ± standard deviation.

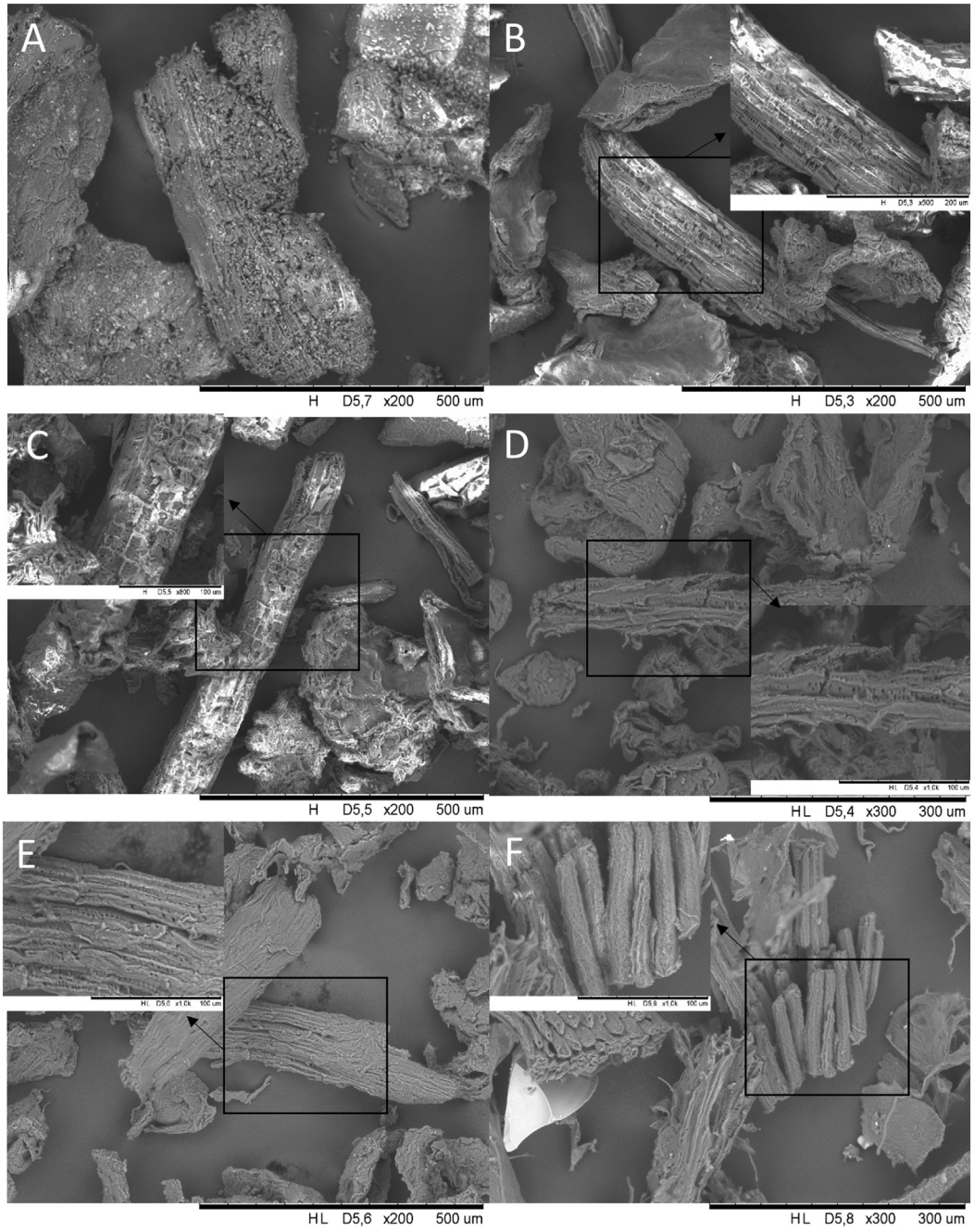

Fig. 3. SEM images of (A) grape pomace *in natura* (×200, scale bar: 500 μm), (B) residue after ethanolic extraction (×200, scale bar: 500 μm), (C) residue after acid extraction (×200, scale bar: 500 μm), (D) after alkaline extraction (×300, scale bar: 300 μm), (E) first bleaching (×200, scale bar: 500 μm), and (F) second bleaching (×300, scale bar: 300 μm).

decreased the thermal stability of cellulose as a result of the dehydration reaction.

In both, fresh grape pomace and cellulose samples, two decomposition peaks were observed near 160 and 220 °C which may be associated with the successive degradation of different lignocellulosic fractions, such as hemicellulose, lignin and pectin, which present low decomposition temperature. However, these peaks were not clear in CNC samples.

CNCs presented less carbonized residues (1.37%) (ashes) when compared to cellulose (22.10%) and fresh (*in natura)* pomace (28.88%) (Table 2), which was probably related to lignin degradation process that persisted up to temperatures higher than 500 °C, due to the higher thermal stability of benzene-propane structure, when compared to polysaccharides, such as cellulose and hemicellulose [23], evidencing the removal of these components from CNCs.

3.2. Characterization of the films

3.2.1. Thickness, moisture content (MC), solubility (Sol), water vapor permeability (WVP), and contact angle (CA°) of nanocomposite films

Thickness, water vapor permeability (WVP) and contact angle (CA) values of the nanocomposites are shown in Table 3. Moisture content (MC) and solubility (Sol) results are shown in supporting information of Table 1.

Film thickness may affect some physical properties, such as water vapor and gas permeability, mechanical properties and opacity. The incorporation of 5, 10 and 15% of CNCs negatively influenced thickness increase of the films ($p < .05$). It is known that a greater thickness is due to higher amount of solids present in the nanocomposites. Machado et al. [56] produced nanocomposites with thickness of 0.15 mm by adding

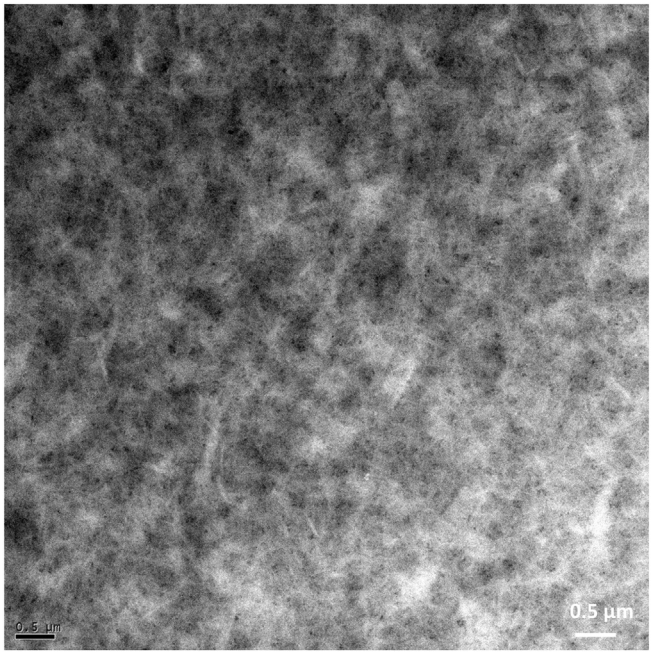

Fig. 4. STEM-DF micrographies of cellulose nanocrystals extracted from grape pomace. Bright contrasts correspond to the cellulose nanocrystals.

0.3% CNCs from coconut fiber in cassava starch films. This value was higher than the observed in this study, probably due to the higher starch content (6%) present in film formulation.

CNC incorporation did not significantly change the moisture content and solubility of nanocomposites ($p > .05$) when compared to the control film. Different results were found by Noshirvani et al. [57]. These authors reported that as CNC content increased from 3% to 20%, the solubility in water of nanocomposites of potato starch/polynilic alcohol/CNC decreased from 20.85% to 11.92%, respectively ($p < .05$). This finding may be associated with the hydrogen bond created between starch hydroxyl groups and CNCs, which leads to the formation of three-dimensional cellulose networks. This 3D generated network limits polymer solubility and leads to network reinforcement, which restricts the movement of low-molecular weight polymers and other compounds towards water [57]. Nanocomposite solubility remained low even with small concentrations of CNCs incorporated in the films

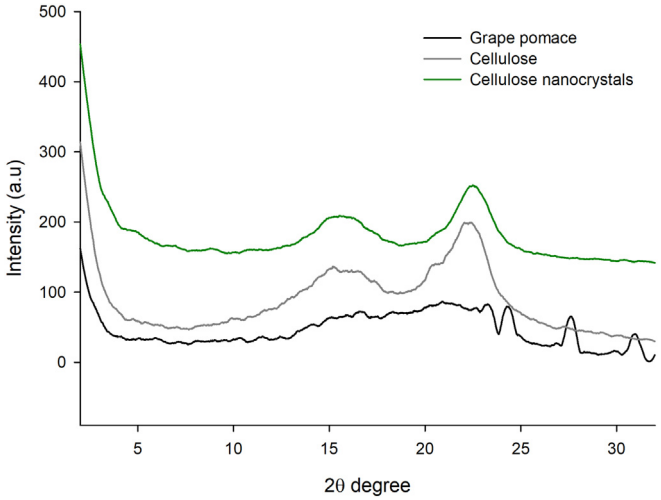

Fig. 5. XRD spectra of grape pomace *in natura*, cellulose and CNC isolates.

(e.g. 12.32% in ST 1% CNCs), i.e., due to good dispersion, even at low concentrations, the addition of CNCs was effective in promoting hydrogen bonds between polymers, able to reduce the interaction between water and film.

As shown in Table 3, regardless the percentage of CNCs added to the ST matrix, WVP significantly decreased ($p < .05$) when compared to the control film. According to Noshirvani et al. [57] the presence of CNC is able to increase the tortuosity of water molecules in the polymeric matrix, and therefore, reducing WVP, as confirmed by our previous XRD results on CNCs.

The permeability of control film was 7.5 ± 0.35 g x h.m.Pa^{-1}, after the reinforcement with CNCs the WVP values decreased. The addition of 1 and 2% CNCs in starch films presented the lowest WVP values (4.25 and 4.55 × 10^{-7} g x h.m.Pa^{-1}), respectively. However, when CNC increased in the nanocomposites, (5%, 10% and 15% CNCs), WVP significantly increased ($p < .05$). Therefore, in those concentrations (1 and 2% CNCs), CNC could well disperse in the ST matrix, providing a tortuosity increase of water molecules in the polymeric matrix, thus decreasing WVP. Balakrishnan, et al. [16] reported that the incorporation of 1 to 4% of cellulose nanofibers (CNF) in starch nanocomposites reduced the WVP, due to the good dispersion of nanofibers in ST based, hence producing strong hydrogen bonding that hinders water molecules to enter into the nanocomposites. However, 3% of CNF presented lower WVP. According to these authors, 4% CNF in starch films presented agglomeration of nanostructures increasing WVP.

The barrier improvement to moisture in polymeric films with CNC incorporation has been shown by Noshirvani et al. [57]. Those authors reported that the incorporation of 3 to 15% was able to reduce WVP, however 20% of CNC in potato starch/polyvinyl alcohol/CNC nanocomposites presented agglomeration of nanostructures increasing WVP, which led to a faster diffusion of water vapor through the film.

Starch is characterized as a hydrophilic polymer [38]. The low value of CA indicates the high wettability capacity of a water drop on the surface of such films. Experimental results listed in Table 3 indicate that the addition of CNCs to ST matrix can significantly increase CA and, therefore, increases the hydrophobicity of nanocomposites in comparison with ST control films. However, this improvement depends on the amount of CNCs: the incorporation of up to 10% CNCs to the matrix led to increased CA. This behavior corresponds to the highly crystalline, hydrophobic characteristics of CNCs, when compared to starch [58]. However, when reinforcement concentration increased to 15% of CNCs, CA value did not differ from that of the control film, which may be attributed to the possible aggregation caused by the higher CNC concentration in the matrix. Therefore, an adequate concentration of CNCs leads to the formation of strong interactions of hydrogen bonds between ST and CNCs, able to increase CA and reduce WVP, as previously observed.

Similar results were found by Slavutsky & Bertuzzi [59], who reported a major hydrophobicity improvement in the surface of nanocomposite films based on ST and 3% CNCs obtained from sugarcane bagasse, when compared to films containing just ST. Similarly, Noshirvani et al. [57] showed CA increase in nanocomposites when CNC content increased from 0 to 20%.

3.2.2. Apparent color and opacity

Table 4 shows surface color properties and the total color difference (ΔE) of composite films. The values of L* and ΔE did not present significant difference after the incorporation of different concentrations of CNCs ($p > .05$); however, a* values decreased and b* values increased with the incorporation of 5, 10 and 15% CNCs, having yellowish hue. Similar behavior of the optical properties of agar films was reported by Shankar & Rhim [60], who evidenced that the incorporation of CNCs (0–5%) as reinforcement material had a significant effect on the color of the films.

Nanocomposites with low CNC concentrations (1 and 2%) were as transparent as the control, but after the addition of higher amounts (5,

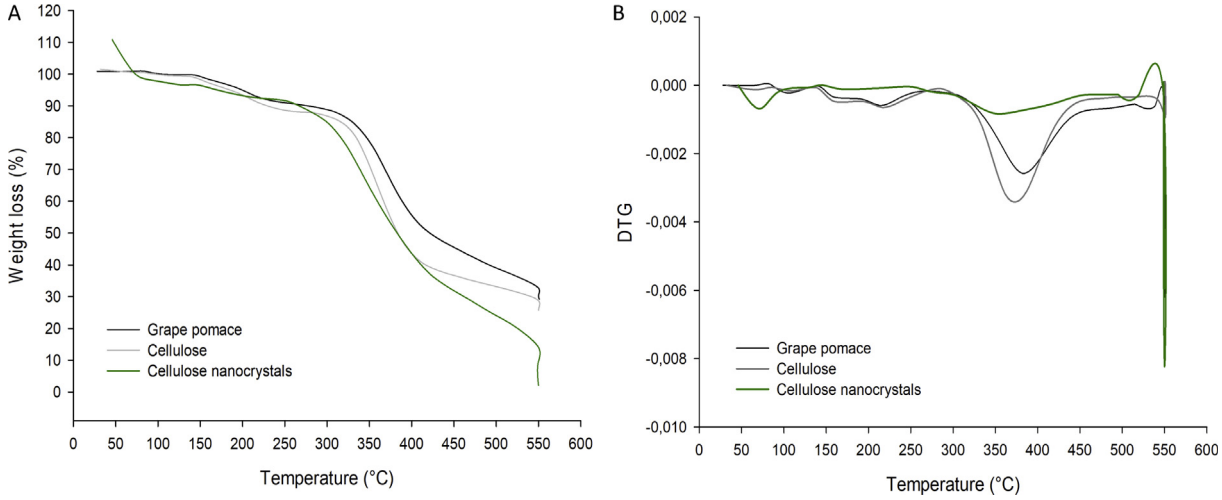

Fig. 6. (A) TG curves and (B) DTG curves of grape pomace *in natura*, cellulose and CNCs isolated from grape pomace.

10 and 15% CNCs), the opacity values of the films increased, thus decreased the transparency of the starch film with the increase of CNC content. According to Li et al. [38] composite films present opacity increase due to the strong interaction between CNCs and the starch matrix, as well as to the light dispersion of added CNCs. The low effect of CNCs on film opacity observed in the present study may be explained by the adequate dispersion of CNCs in the starch matrix. Similar results were found by Oliveira et al. [61] who observed only significant increase of film opacity when 10% CNC was added to agar films. In addition to its high transparency and excellent dispersion at the nanoscale, potato starch/CNCs films are UV resistant, which has been found by other authors [62].

3.2.3. Scanning electron microscopy (SEM)

SEM images of the surface and cross-section of the films are shown in Fig. 7. All films presented characteristics of homogenous, continuous, smooth surface without pores or granules and bubbles free (Fig. 7b), indicating good CNC dispersion in ST matrix.

SEM micrograph of the cross-section of the control film (Fig. 7a – Control) shows a heterogeneous surface with discontinuous gaps in the matrix, which may explain the high WVP found in these films compared to films added by CNCs, since the formation of paths may facilitate the passage of water vapor, as previously reported.

It is evident that the roughness of the cross-section of the films increases when CNCs are added to the ST based film. The smaller concentrations of CNCs added, 1 and 2% provided rough structures, although without phase separation (Fig. 7a – ST 1% CNCs and ST 2% CNCs). In addition, the homogeneity of the films may be linked to the lowest WVP values found in the films added of the the lowest concentrations of CNCs. These results indicate excellent compatibility between both components, starch and CNCs, mainly in low amounts.

However, films added of 5, 10 and 15% CNCs presented phase separation along the cross-section, with smoother and denser layer and another rougher layer (detail shown by the arrow in the corresponding figures) (Fig. 7a – ST 5% CNCs, ST 10% CNCs and ST 15% CNCs). These films, added of the bigger concentrations of CNCs, are more permeable and more opaque, which are characteristics ascribed to aggregations of nanocrystals [63].

Nessi et al. [64] observed that the incorporation of 1.5 and 2.5% of CNCs in starch films produced homogeneous and smooth nanocomposites film. When adding 5 and 10% CNC, small voids and discontinuities appear in the nanocomposite. The authors report that this roughness can come from an aggregation of particles, making the materials less homogeneous.

Liu et al. [65] studied the effect of the incorporation of CNCs, obtained from acid hydrolysis of bleached flax in ST films. They reported that the incorporation of sulfate groups during hydrolysis resulted in a negatively-charged cellulose surface. At this stage, an anionic stabilization occurs through attraction/repulsion electric forces and thus, the aqueous suspension formed by CNCs becomes stable and uniform. Also, according to those authors, when the mixture of ST and CNCs occurs, followed by heating of the solution and subsequent evaporation

Table 3
Effect of CNC concentration on the thickness, moisture content (MC), solubility (Sol), water vapor permeability (WVP), and contact angle (CA°) of nanocomposite films.

Film	Thickness (mm)	Permeability × 10^{-7} (WVP) (g h^{-1} m^{-1} Pa^{-1})	Contact angle (CA) (°)
Control	0.08 ± 0.01^{c}	7.5 ± 0.35^{a}	26.10 ± 5.50^{b}
ST 1% CNCs	0.08 ± 0.01^{c}	4.25 ± 0.23^{d}	35.36 ± 7.91^{a}
ST 2% CNCs	0.08 ± 0.01^{c}	4.55 ± 0.22^{d}	35.02 ± 3.51^{a}
ST 5% CNCs	0.09 ± 0.01^{b}	6.63 ± 0.15^{b}	36.79 ± 6.32^{a}
ST 10% CNCs	0.10 ± 0.01^{ab}	5.33 ± 0.36^{c}	33.84 ± 4.82^{a}
ST 15% CNCs	0.11 ± 0.01^{a}	6.02 ± 0.11^{bc}	29.54 ± 5.46^{ab}

Values represent the mean ± standard deviation.
Values in a column having different superscripts are significantly different ($p < .05$).

Table 2
Thermal behavior of grape pomace *in natura*, cellulose and CNCs isolated from grape pomace.

Samples	T_{onset} (°C)	T_{max} (°C)	% of degradation at T_{max}	Ash content at 550 °C
Grape pomace *in natura*	230 ± 9.61^{a}	381 ± 7.64^{a}	61 ± 2.65^{a}	28.88 ± 0.51^{a}
Cellulose	232 ± 2.65^{a}	365 ± 9.64^{ab}	57 ± 4.58^{a}	22.10 ± 3.58^{b}
Cellulose nanocrystals	203 ± 23.69^{b}	348 ± 9.29^{b}	63 ± 1.53^{a}	1.37 ± 2.16^{c}

Values represent the mean ± standard deviation.
Values in a column having different superscripts are significantly different ($p < .05$).

Table 4
Apparent color and opacity of ST/CNCs composite films.

Film	L*	a*	b*	ΔE	Opacity (%)
Control	93.75 ± 0.26[a]	−0.09 ± 0.00[c]	−0.06 ± 0.02[c]	–	4.28 ± 0.47[b]
ST 1% CNCs	94.51 ± 0.18[a]	−0.10 ± 0.00[c]	−0.08 ± 0.03[c]	0.76 ± 0.44[a]	4.27 ± 0.36[b]
ST 2% CNCs	94.54 ± 0.16[a]	−0.09 ± 0.01[c]	−0.08 ± 0.05[c]	0.79 ± 0.16[a]	4.38 ± 0.50[b]
ST 5% CNCs	93.75 ± 0.95[a]	−0.12 ± 0.01[ab]	0.23 ± 0.11[b]	0.81 ± 0.32[a]	5.48 ± 0.23[a]
ST 10% CNCs	94.19 ± 0.15[a]	−0.11 ± 0.00[bc]	0.42 ± 0.07[ab]	0.59 ± 0.15[a]	6.35 ± 0.09[a]
ST 15% CNCs	94.18 ± 0.01[a]	−0.13 ± 0.00[a]	0.45 ± 0.05[a]	0.69 ± 0.20[a]	5.79 ± 0.14[a]

Values represent the mean ± standard deviation.
Values in a column having different superscripts are significantly different ($p < .05$).

in the drying of the films, CNCs may be rearranged with water evaporation. Even though the films presented smooth, transparent and uniform aspects, SEM showed that when nanoparticles were incorporated, the films presented CNC layers, evidenced by 50,000× magnification. In addition, layer thickness increase was observed as CNC concentration increased (5 to 20%) and those authors did not observe strong interactions between CNCs and the ST matrix.

Cao et al. [66] obtained CNCs from hemp homogenously incorporated to plasticized ST (10 to 30%). The compatibility of the materials was attributed to factors such as (i) chemical similarities between starch and cellulose, (ii) interaction of hydrogen bonds between CNCs and the matrix and (iii) effect of CNC nanometric size.

3.2.4. Mechanical properties

Data on the effect of different CNC concentrations incorporated in ST films are presented in Fig. 8. In general, there was a significant increase of tensile strength (TS) (Fig. 8A) and Young's modulus (YM) (Fig. 8C), whereas elongation at break (%) (EB) (Fig. 8B) decreased in films with higher incorporations of CNCs (ST 5% CNCs, ST 10% CNCs and ST 15% CNCs).

The values of TS significantly increased with CNC incorporation to 24.64, 21.47 and 21.38 MPa, for the films ST 5% CNCs, ST 10% CNCs and ST 15% CNCs, respectively, which presented significant difference in relation to the Control films, ST 1% CNCs and ST 2% CNCs. However, ST 1% CNCs and ST 2% CNCs films did not significantly differ from the control film. (14.88, 13.03 and 16.28 MPa, respectively). The TS values of nanocomposite films can be compared to some commercial petroleum based films, such as *low-density polyethylene* (*LDPE*) (8–10 MPa), *polypropylene* (PP) (27–98 MPa), polystyrene (PS) (31–49 MPa) and *polylactic acid* (PLA) (45 MPa) [67].

EB was higher in the control film (13.11%) with significant difference in relation to the nanocomposites. The addition of small concentrations of CNCs, ST 1% CNCs and ST 2% CNCs, was able to decrease EB (8.09 and 10.29%, respectively), whereas ST 5% CNCs, ST 10% CNCs and ST 15% CNCs films presented lower values of EB, 4.26, 4.46 and 3.66%, respectively.

One the other hand, YM increased in ST 5% CNCs, ST 10% CNCs and ST 15% CNCs nanocomposites (20.96, 17.68 and 17.22 MPa, respectively). The high values of YM may be explained by the reinforcement effect caused by CNC in higher concentrations, may be attributed to the strong

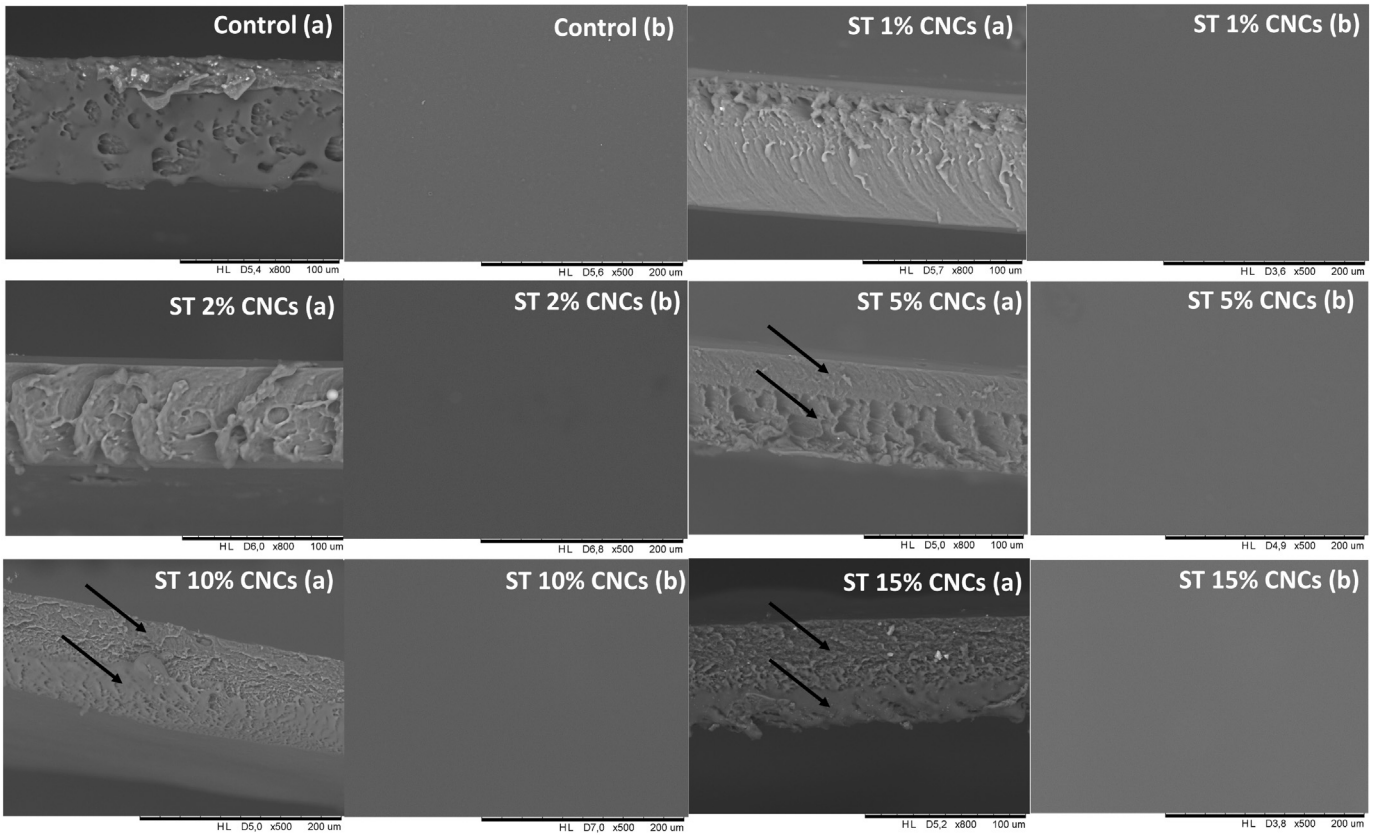

Fig. 7. Scanning electron microscopy images of (a) cross-section and (b) surface for pure starch (control), and starch composite films containing: 1 (ST 1% CNCs), 2 (ST 2% CNCs), 5 (ST 5% CNCs), 10 (ST 10% CNCs) and 15 (ST 15% CNCs) wt% CNWs.

interaction of hydrogen bonds between CNC and ST molecules. However, the decrease of EB indicates that CNC incorporation restricts the movement of ST matrix due to the similarities of chemical structure of cellulose and ST that promote strong interactions between them [66].

The results show that the incorporation of CNCs from 5% of the CNCs caused a mechanical reinforcement. The heterogeneous micrograph of the nanocomposites films caused by the aggregation of the CNCs seemed not affect the mechanical and barrier properties, as shown earlier, also noticed previously by Silva et al. [63] on starch films added with CNCs; but instead, these properties have improved with the incorporation of nanocrystals.

Gray et al. [13] observed that the mechanical properties of resistance of nanocomposites of thermoplastic starch considerably improved by CNC addition. However, those authors verified poor dispersion of greater concentrations of CNCs in the starch matrix and consequently, less resistance of the films.

Some studies described the effects of CNCs improving both, YM and TS but reducing EB. Yadav et al. [67] observed increase of TS and decrease of EB in alginate/CNCs films with 5 wt% CNCs, that exhibited greater TS (35.5 MPa) than pure alginate films (25.6 MPa) and greater EB (14.3 MPa) than pure alginate films (17.1 MPa).

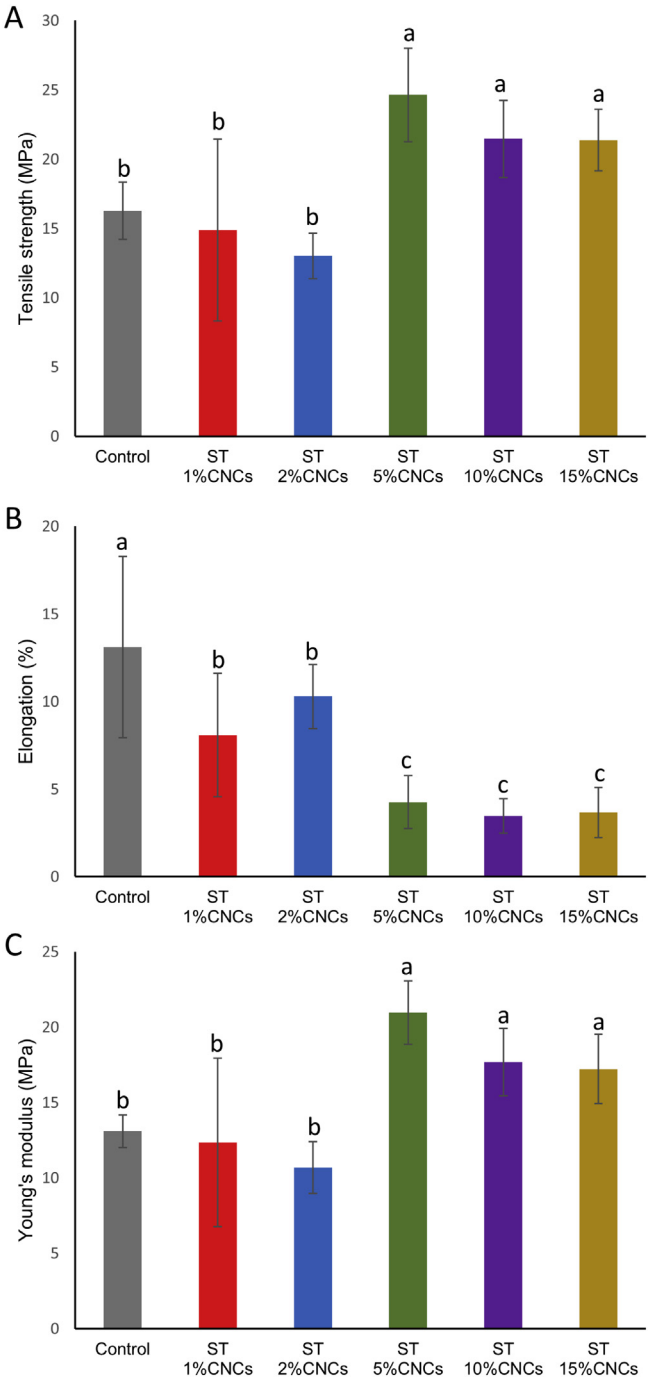

Fig. 8. Values of mechanical properties for ST/CNCs nanocomposites. Tensile strength (MPa) (A), Elongation (%) (B) and Young's modulus (MPa) (C) of Control, ST 1%, ST 2% CNCs, ST 5% CNCs, ST 10% CNCs and ST 15% CNCs. Values represent the mean ± standard deviation. Values in columns with different letters are significantly different ($p < .05$).

3.2.5. X-ray diffraction (XRD)

The X-ray diffraction patterns were carried out based on the addition of CNC content, and the correspondent diffractograms are shown in Fig. 9. The control film presented a typical pattern of type β crystallinity, with peaks at 2θ = 5.9 (characteristic of type B polymorphous), 2θ = 17° (characteristic of Type A and B polymorphous and 2θ = 22.5° (characteristic of type B polymorphous). These results are consistent with previous studies by Talja [68] and Li et al. [38]. According to Rico et al. [17] and Li et al. [38] the crystalline structure of ST may be attributed to two types of crystallinity: residual crystallinity and crystallinity induced by the process. Residual crystallinity is caused by the incomplete melting of native ST during processing or even by the reorganization of ST molecular chains in their native arrangements. On the other hand, induced crystallinity is caused by crystallization of amylose chains complexed with plasticizers (such as glycerol) in unique helicoidal structures, that can be induced during heating, where strong interactions between OH groups from ST molecular chains are replaced by hydrogen bonds formed between ST and the plasticizer [17,38]

Three well-defined diffraction peaks were found in nanocomposites films, located at 2θ = 16–17°, 19° and 22.5°. The peaks at 2θ = 16–17° and 2θ = 22.5° may be attributed to cellulose I typical structure, as observed in previous CNC analysis. The intensity of those peaks significantly increased with the increase of CNC content. In ST 10% CNCs and ST 15% CNCs films these peaks are more intense and may be attributed to the highly enriched cellulose regions, indicating that high degree of crystallinity. Rico et al. [17] and Li et al. [38] also observed intensity increment of these peaks with increasing CNC content. The physical and

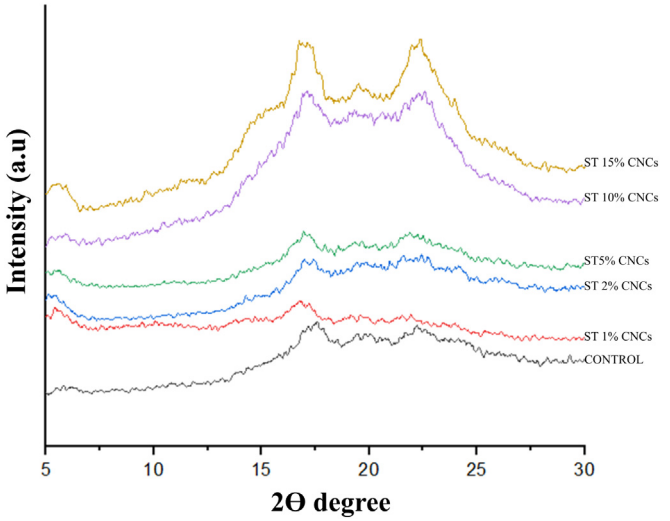

Fig. 9. XRD analysis of ST/CNCs nanocomposites. – Control, -- ST 1%, - ST 2% CNCs, -- ST 5% CNCs, -- ST 10% CNCs, and -- ST 15% CNCs.

Table 5
T_{onset} (°C) and T_{max} (°C) of ST/CNCs composite films.

Film	T_{onset} (°C)	T_{max} (°C)
Control	307 ± 3.21^{c}	335 ± 2.65^{ab}
ST 1% CNCs	303 ± 5.20^{c}	324 ± 0.58^{c}
ST 2% CNCs	294 ± 6.93^{bc}	336 ± 3.06^{a}
ST 5% CNCs	287 ± 3.51^{b}	334 ± 5.29^{ab}
ST 10% CNCs	281 ± 6.03^{b}	328 ± 0.58^{bc}
ST 15% CNCs	266 ± 6.03^{a}	328 ± 1.53^{bc}

Values represent the mean ± standard deviation.
Values in a column having different superscripts are significantly different ($p < 0.05$).

mechanical properties of the nanocomposites were changed due to the crystalline morphology and crystal forms of CNCs [67].

3.2.6. Thermogravimetric analysis (TGA)

The thermogravimetric stability of the films was assessed by TGA. The values of T_{onset} and T_{max} are listed in Table 5. Fig. 10a shows the thermogravimetric curve (TG) and Fig. 10b the derivative thermogravimetric curve (DTG). It is observed that TG curves evidenced essentially the same behavior, indicating a similar degradation mechanism with temperature increase.

Weight loss during heating of ST materials occurred mainly in two stages. First, there was a drop up to near 250 °C, associated to evaporation of low molecular weight molecules (first water and then glycerol). In this stage, the first peak is associated with the process of water evaporation, characteristic phenomenon of a polysaccharide of hydrophilic nature under temperature increase from 82 to 92 °C. The second peak, around 200–250 °C, could be attributed to the presence of glycerol and varies from 178 °C to 243 °C. The second degradation stage occurred in the range from 270 to 400 °C and may correspond to the ST thermal decomposition coupled to CNC degradation that occurs at similar temperatures [17].

Control, ST 1% CNCs and ST 2% CNCs films presented higher values of T_{onset} (307 °C, 303 °C and 294 °C, respectively), but when CNC was added in concentrations of 5–15% those values decreased. T_{max} was higher in ST 2% CNCs film, however, it was not significantly different from control and ST 5% CNCs films. Higher CNC concentrations incorporated in ST 10% CNCs and ST 15% CNCs films presented lower T_{max}, but not significantly different from ST 1% CNCs film. Although T_{max} presented a similar value for all composites, with difference of just 9 °C, in general, nanocomposites did not present improved thermal stability when compared to pure ST film.

4. Conclusions

It was possible to show the potential of grape pomace to be used as raw material for obtaining cellulose. The pre-treatment applied was a successful approach to eliminate initial non-cellulosic components of the pomace and obtaining a cellulosic material, with values for CrI 64% and yield of 12% in cellulose.

Cellulose nanocrystals were extracted from cellulose by acid hydrolysis led to the production of nano structures shown by STEM. XRD results showed CNCs exhibited crystalline structure of cellulose I, CrI of 71%, yield 70% and good thermal stability shown by TGA, important features for use of these nanocomposites (CNCs) in polymeric matrices, allowing their application as reinforcement materials.

CNCs incorporation was able to decrease WVP values in starch films. Films with 5 to 15% CNCs appeared more opaque and might be applied in packaging of foods that are easily degraded when exposed to light. The heterogeneous micrograph of the nanocomposites with 5 to 15% did not affect the mechanical and barrier properties. These films showed greater tensile strength and Young's modulus; therefore, stronger network structure possibly cause by the interaction of CNCs and the starch matrix. In general, nanocomposites did not present improved thermal stability when compared to pure starch film. Such results indicate that the films incorporated of 5 to 15% CNC have better potential for future applications in the field of food packaging.

Supplementary data to this article can be found online at https://doi.org/10.1016/j.ijbiomac.2020.05.046.

Author statement

Caroline C.S. Coelho: Data curation, Investigation, Formal analysis, Writing - Original draft preparation; *Raysa Brandão Soares Silva*: Investigation, data curation; *Carlos W.P. Carvalho*: Resources and Reviewing; *André Linhares Rossi*: Data curation, Reviewing; *José A. Teixeira*: Writing - Reviewing; *Otniel Freitas-Silva*: Supervision, Writing - Reviewing and Editing Project administration; *Lourdes M.C. Cabral*: Conceptualization, Methodology, Resources and Supervision.

Acknowledgements

The authors are grateful for financial support provided by FAPERJ - Fundação de Amparo à Pesquisa do Estado do Rio de Janeiro, Brazil (E-26.202749/2018), the National Council for Scientific and Technological Development – CNPq (311936/2018-0), and the Coordenação

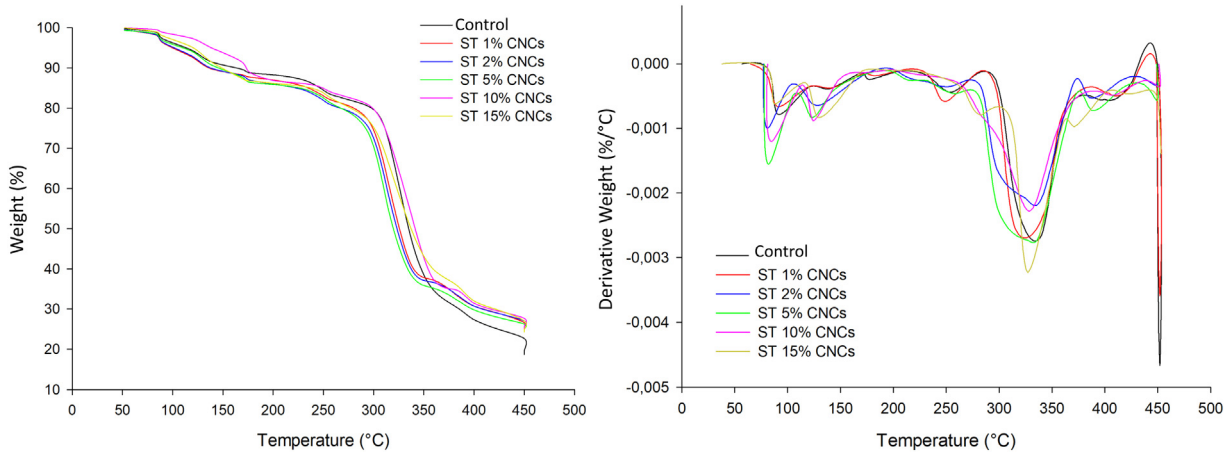

Fig. 10. Thermogravimetric analysis (TGA) and derivative thermogravimetric (DTG) curves for ST/CNCs nanocomposites. – Control, -- ST 1% CNCs, - ST 2% CNCs, -- ST 5% CNCs, -- ST 10% CNCs and -- ST 15% CNCs.

de Aperfeiçoamento Pessoal do Ensino Superior (CAPES). The support during transmission electron microscopy analyses provided by the LABNANO/CBPF is also very much appreciated.

References

[1] C.C.S. Coelho, M.A. Cerqueira, R.N. Pereira, L.M. Pastrana, O. Freitas-Silva, A.A. Vicente, L.M.C. Cabral, J.A. Teixeira, Effect of moderate electric fields in the properties of starch and chitosan films reinforced with microcrystalline cellulose, Carbohydr. Polym. 174 (2017) 1181–1191, https://doi.org/10.1016/j.carbpol.2017.07.007.

[2] C.C.S. Coelho, R.V. Tonon, L.M.C. Cabral, O. Freitas-Silva, M. Michelin, A.A. Vicente, J.A. Teixeira, M.A. Cerqueira, C. Gonçalves, L.M. Pastrana, Cellulose nanocrystals from grape pomace: production, properties and cytotoxicity assessment, Carbohydr. Polym. 192 (2018) 327–336, https://doi.org/10.1016/j.carbpol.2018.03.023.

[3] L.F. Ballesteros, M. Michelin, A.A. Vicente, J.A. Teixeira, M.Â. Cerqueira, Use of lignocellulosic materials in bio-based packaging, Lignocellul. Mater. Their Use Bio-Based Packag, Springer, Cham 2018, pp. 65–85, https://doi.org/10.1007/978-3-319-92940-8.

[4] V. Katiyar, S.S. Gaur, A.K. Pal, A. Kumar, Properties of plastics for packaging applications, in: A.A. Press (Ed.), Polym. Packag. Appl, 1st ed. 2014, pp. 3–34.

[5] P.M. Visakh, A.P. Mathew, K. Oksman, S. Thomas, Starch-based bionanocomposites: processing and properties, in: Y. Habibi, L.A. Lucia (Eds.),Polysacch. Build. Blocks a Sustain. Approach to Dev. Renew. Biomater, 1st ed. 2012, pp. 287–306, https://doi.org/10.1002/9781118229484.

[6] R. Thakur, P. Pristijono, C.J. Scarlett, S.P. Singh, Q.V. Vuong, Starch-based films: major factors affecting their properties, Int. J. Biol. Macromol. 132 (2019) 1079–1089, https://doi.org/10.1016/j.ijbiomac.2019.03.190.

[7] L. Dai, J. Zhang, F. Cheng, Effects of starches from different botanical sources and modification methods on physicochemical properties of starch-based edible films, Int. J. Biol. Macromol. 132 (2019) 897–905, https://doi.org/10.1016/j.ijbiomac.2019.03.197.

[8] A. Shi, L. Wang, D. Li, B. Adhikari, Characterization of starch films containing starch nanoparticles, Carbohydr. Polym. 96 (2013) 593–601, https://doi.org/10.1016/j.carbpol.2012.12.042.

[9] P. Balakrishnan, S. Gopi, V.G. Geethamma, N. Kalarikkal, S. Thomas, Cellulose nanofiber vs nanocrystals from pineapple leaf fiber: a comparative studies on reinforcing efficiency on starch nanocomposites, Macromol. Symp. 380 (2018) 1–7, https://doi.org/10.1002/masy.201800102.

[10] R.R. Koshy, S.K. Mary, L.A. Pothan, S. Thomas, Soy protein- and starch-based green composites/nanocomposites: preparation, properties, and applications, in: Springer India (Ed.), Eco-Friendly Polym. Nanocomposites Process. Prop 2015, pp. 433–467, https://doi.org/10.1007/978-81-322-2470-9.

[11] F. Mohanty, S.K. Swain, Nano silver embedded starch hybrid graphene oxide sandwiched poly(ethylmethacrylate) for packaging application, Nano-Structures and Nano-Objects 18 (2019), 100300. https://doi.org/10.1016/j.nanoso.2019.100300.

[12] L. Brinchi, F. Cotana, E. Fortunati, J.M. Kenny, Production of nanocrystalline cellulose from lignocellulosic biomass: technology and applications, Carbohydr. Polym. 94 (2013) 154–169, https://doi.org/10.1016/j.carbpol.2013.01.033.

[13] N. Gray, Y. Hamzeh, A. Kaboorani, A. Abdulkhani, Influence of cellulose nanocrystal on strength and properties of low density polyethylene and thermoplastic starch composites, Ind. Crop. Prod. 115 (2018) 298–305, https://doi.org/10.1016/j.indcrop.2018.02.017.

[14] K. González, O. Guaresti, T. Palomares, A. Alonso-Varona, A. Eceiza, N. Gabilondo, The role of cellulose nanocrystals in biocompatible starch-based clicked nanocomposite hydrogels, Int. J. Biol. Macromol. 143 (2020) 265–272, https://doi.org/10.1016/j.ijbiomac.2019.12.050.

[15] K. Vaezi, G. Asadpour, S.H. Sharifi, Bio nanocomposites based on cationic starch reinforced with montmorillonite and cellulose nanocrystals: fundamental properties and biodegradability study, Int. J. Biol. Macromol. 146 (2020) 374–386, https://doi.org/10.1016/j.ijbiomac.2020.01.007.

[16] P. Balakrishnan, M.S. Sreekala, M. Kunaver, M. Huskić, S. Thomas, Morphology, transport characteristics and viscoelastic polymer chain confinement in nanocomposites based on thermoplastic potato starch and cellulose nanofibers from pineapple leaf, Carbohydr. Polym. 169 (2017) 176–188, https://doi.org/10.1016/j.carbpol.2017.04.017.

[17] M. Rico, S. Rodríguez-Llamazares, L. Barral, R. Bouza, B. Montero, Processing and characterization of polyols plasticized-starch reinforced with microcrystalline cellulose, Carbohydr. Polym. 149 (2016) 83–93, https://doi.org/10.1016/j.carbpol.2016.04.087.

[18] M.R. Sucaldito, D.H. Camacho, Characteristics of unique HBr-hydrolyzed cellulose nanocrystals from freshwater green algae (Cladophora rupestris) and its reinforcement in starch-based film, Carbohydr. Polym. 169 (2017) 315–323, https://doi.org/10.1016/j.carbpol.2017.04.031.

[19] A.P. Mathew, A. Dufresne, Morphological investigation of nanocomposites from sorbitol plasticized starch and tunicin whiskers, Biomacromolecules 3 (2002) 609–617, https://doi.org/10.1021/bm0101769.

[20] F. Jiang, Y. Lo Hsieh, Cellulose nanocrystal isolation from tomato peels and assembled nanofibers, Carbohydr. Polym. 122 (2015) 60–68, https://doi.org/10.1016/j.carbpol.2014.12.064.

[21] M. El Achaby, Z. Kassab, A. Aboulkas, C. Gaillard, A. Barakat, Reuse of red algae waste for the production of cellulose nanocrystals and its application in polymer nanocomposites, Int. J. Biol. Macromol. 106 (2018) 681–691, https://doi.org/10.1016/j.ijbiomac.2017.08.067.

[22] J. Marett, A. Aning, E.J. Foster, The isolation of cellulose nanocrystals from pistachio shells via acid hydrolysis, Ind. Crop. Prod. 109 (2017) 869–874, https://doi.org/10.1016/j.indcrop.2017.09.039.

[23] K.S. Prado, M.A.S. Spinacé, Isolation and characterization of cellulose nanocrystals from pineapple crown waste and their potential uses, Int. J. Biol. Macromol. 122 (2019) 410–416, https://doi.org/10.1016/j.ijbiomac.2018.10.187.

[24] F. Luzi, E. Fortunati, D. Puglia, M. Lavorgna, C. Santulli, J.M. Kenny, L. Torre, Optimized extraction of cellulose nanocrystals from pristine and carded hemp fibres, Ind. Crop. Prod. 56 (2014)https://doi.org/10.1016/j.indcrop.2014.03.006.

[25] A.A. Oun, J.W. Rhim, Isolation of cellulose nanocrystals from grain straws and their use for the preparation of carboxymethyl cellulose-based nanocomposite films, Carbohydr. Polym. 150 (2016)https://doi.org/10.1016/j.carbpol.2016.05.020.

[26] H.M. Ng, L.T. Sin, T.T. Tee, S.T. Bee, D. Hui, C.Y. Low, A.R. Rahmat, Extraction of cellulose nanocrystals from plant sources for application as reinforcing agent in polymers, Compos. Part B Eng. 75 (2015)https://doi.org/10.1016/j.compositesb.2015.01.008.

[27] M. Martínez-Sanz, A. Lopez-Rubio, J.M. Lagaron, Optimization of the nanofabrication by acid hydrolysis of bacterial cellulose nanowhiskers, Carbohydr. Polym. 85 (2011) 228–236, https://doi.org/10.1016/j.carbpol.2011.02.021.

[28] Q. Jiang, X. Xing, Y. Jing, Y. Han, Preparation of cellulose nanocrystals based on waste paper via different systems, Int. J. Biol. Macromol. 149 (2020) 1318–1322, https://doi.org/10.1016/j.ijbiomac.2020.02.110.

[29] M. Yadav, F.C. Chiu, Cellulose nanocrystals reinforced κ-carrageenan based UV resistant transparent bionanocomposite films for sustainable packaging applications, Carbohydr. Polym. 211 (2019) 181–194, https://doi.org/10.1016/j.carbpol.2019.01.114.

[30] M. Yadav, Y.K. Liu, F.C. Chiu, Fabrication of cellulose nanocrystal/silver/alginate bionanocomposite films with enhanced mechanical and barrier properties for food packaging application, Nanomaterials 9 (2019) 1523, https://doi.org/10.3390/nano9111523.

[31] C.J. Chirayil, L. Mathew, S. Thomas, Review of recent research in nano cellulose preparation from different lignocellulosic fibers, Rev. Adv. Mater. Sci. 37 (2014).

[32] H.M.C. Azeredo, M.F. Rosa, L.H.C. Mattoso, Nanocellulose in bio-based food packaging applications, Ind. Crop. Prod. (2017)https://doi.org/10.1016/j.indcrop.2016.03.013.

[33] M. Thakur, A. Sharma, V. Ahlawat, M. Bhattacharya, S. Goswami, Process optimization for the production of cellulose nanocrystals from rice straw derived α-cellulose, Mater. Sci. Energy Technol. 3 (2020) 328–334, https://doi.org/10.1016/j.mset.2019.12.005.

[34] Y. Lo Hsieh, Cellulose nanocrystals and self-assembled nanostructures from cotton, rice straw and grape skin: a source perspective, J. Mater. Sci. 48 (2013) 7837–7846, https://doi.org/10.1007/s10853-013-7512-5.

[35] R. Moriana, F. Vilaplana, M. Ek, Cellulose nanocrystals from forest residues as reinforcing agents for composites: a study from macro- to nano-dimensions, Carbohydr. Polym. 139 (2016) 139–149, https://doi.org/10.1016/j.carbpol.2015.12.020.

[36] M. Smyth, A. García, C. Rader, E.J. Foster, J. Bras, Extraction and process analysis of high aspect ratio cellulose nanocrystals from corn (Zea mays) agricultural residue, Ind. Crop. Prod. 108 (2017) 257–266, https://doi.org/10.1016/j.indcrop.2017.06.006.

[37] P. Lu, Y. Lo Hsieh, Cellulose isolation and core-shell nanostructures of cellulose nanocrystals from chardonnay grape skins, Carbohydr. Polym. 87 (2012) 2546–2553, https://doi.org/10.1016/j.carbpol.2011.11.023.

[38] M. Li, X. Tian, R. Jin, D. Li, Preparation and characterization of nanocomposite films containing starch and cellulose nanofibers, Ind. Crop. Prod. 123 (2018) 654–660, https://doi.org/10.1016/j.indcrop.2018.07.043.

[39] B. Cuq, N. Gontard, J.L. Cuq, S. Guilbert, Functional properties of myofibrillar protein-based biopackaging as affected by film thickness, J. Food Sci. 61 (1996) 580–584, https://doi.org/10.1111/j.1365-2621.1996.tb13163.x.

[40] V. Guillard, B. Broyart, C. Bonazzi, S. Guilbert, N. Gontard, Preventing moisture transfer in a composite food using edible films: experimental and mathematical study, J. Food Sci. 68 (2003) 2267–2277, https://doi.org/10.1111/j.1365-2621.2003.tb05758.x.

[41] T.H. McHugh, R. Avena-Bustillos, J.M. Krochta, Hydrophilic edible films: modified procedure for water vapor permeability and explanation of thickness effects, J. Food Sci. 58 (1993) 899–903, https://doi.org/10.1111/j.1365-2621.1993.tb09387.x.

[42] D.Y. Kwok, a.W. Neumann, Contact Angle Measurement and Contact Angle Interpretation, 1999https://doi.org/10.1016/S0001-8686(98)00087-6.

[43] Y. Alparslan, T. Baygar, T. Baygar, H. Hasanhocaoglu, C. Metin, Effects of gelatin-based edible films enriched with laurel essential oil on the quality of rainbow trout (Oncorhynchus mykiss) fillets during refrigerated storage, Food Technol. Biotechnol. 52 (2014) 325–333.

[44] A. Casariego, B.W.S. Souza, M.A. Cerqueira, J.A. Teixeira, L. Cruz, R. Díaz, A.A. Vicente, Chitosan/clay films' properties as affected by biopolymer and clay micro/nanoparticles' concentrations, Food Hydrocoll. 23 (2009) 1895–1902, https://doi.org/10.1016/j.foodhyd.2009.02.007.

[45] D.M. do Nascimento, A.F. Dias, C.P. de Araújo Junior, M. de F. Rosa, J.P.S. Morais, M.C.B. de Figueirêdo, A comprehensive approach for obtaining cellulose nanocrystal from coconut fiber. Part II: environmental assessment of technological pathways, Ind. Crop. Prod. 93 (2016) 58–65, https://doi.org/10.1016/j.indcrop.2016.02.063.

[46] J. Xie, C.-Y. Hse, C.F. De Hoop, T. Hu, J. Qi, T.F. Shupe, Isolation and characterization of cellulose nanofibers from bamboo using microwave liquefaction combined with chemical treatment and ultrasonication, Carbohydr. Polym. 151 (2016) 725–734, https://doi.org/10.1016/j.carbpol.2016.06.011.

[47] M. Demirkol, Z. Tarakci, Effect of grape (Vitis labrusca L.) pomace dried by different methods on physicochemical, microbiological and bioactive properties of yoghurt, Food Sci. Technol. 97 (2018) 770–777, https://doi.org/10.1016/j.lwt.2018.07.058. This.

[48] F.M. Pelissari, P.J.D.A. Sobral, F.C. Menegalli, Isolation and characterization of cellulose nanofibers from banana peels, Cellulose 21 (2014) 417–432, https://doi.org/10.1007/s10570-013-0138-6.

[49] N.F. Souza, Processos de obtenção de nanocelulose a partir das fibras da prensagem do mesocarpo do dendê, universidade federal do ceará, 2014.

[50] J.X. Sun, X.F. Sun, H. Zhao, R.C. Sun, Isolation and characterization of cellulose from sugarcane bagasse, Polym. Degrad. Stab. 84 (2004) 331–339, https://doi.org/10.1016/j.polymdegradstab. 2004.02.008.

[51] A. Dufresne, D. Dupetre, M.R. Vignon, Cellulose microfibrils from potato tuber cells: processing and characterization of starch–cellulose microfibril composites, J. Appl. Polym. Sci. 76 (2000) 2080–2092.

[52] R. Li, J. Fei, Y. Cai, Y. Li, J. Feng, J. Yao, Cellulose whiskers extracted from mulberry: a novel biomass production, Carbohydr. Polym. 76 (2009) 94–99, https://doi.org/10.1016/j.carbpol.2008.09.034.

[53] Z. Wang, Z. Yao, J. Zhou, M. He, Q. Jiang, S. Li, Y. Ma, M. Liu, S. Luo, Isolation and characterization of cellulose nanocrystals from pueraria root residue, Int. J. Biol. Macromol. (2018)https://doi.org/10.1016/j.ijbiomac.2018.07.055.

[54] E. Espino, M. Cakir, S. Domenek, A.D. Román-gutiérrez, N. Belgacem, J. Bras, Isolation and Characterization of Cellulose Nanocrystals From Industrial By-products of Agave Tequilana and Barley, 62, 2014 552–559.

[55] M. El Achaby, N. El Miri, H. Hannache, S. Gmouh, H. Ben youcef, A. Aboulkas, Production of cellulose nanocrystals from vine shoots and their use for the development of nanocomposite materials, Int. J. Biol. Macromol. 117 (2018) 592–600, https://doi.org/10.1016/j.ijbiomac.2018.05.201.

[56] Bruna Aparecida Souza Machado, I.L. Nunes, F.V. Pereira, J.I. Druzian, Desenvolvimento e avaliação da eficácia de filmes biodegradáveis de amido de mandioca com nanocelulose como reforço e com extrato de erva-mate como aditivo antioxidante, Ciência Rural 42 (2012) 2085–2091.

[57] N. Noshirvani, W. Hong, B. Ghanbarzadeh, H. Fasihi, R. Montazami, Study of cellulose nanocrystal doped starch-polyvinyl alcohol bionanocomposite films, Int. J. Biol. Macromol. 107 (2018) 2065–2074, https://doi.org/10.1016/j.ijbiomac.2017.10.083.

[58] X. Cao, Y. Chen, P.R. Chang, M. Stumborg, M.A. Huneault, Green composites reinforced with hemp nanocrystals in plasticized starch, J. Appl. Polym. Sci. 109 (2008) 3804–3810, https://doi.org/10.1002/app.

[59] A.M. Slavutsky, M.A. Bertuzzi, Water barrier properties of starch films reinforced with cellulose nanocrystals obtained from sugarcane bagasse, Carbohydr. Polym. 110 (2014) 53–61, https://doi.org/10.1016/j.carbpol.2014.03.049.

[60] S. Shankar, J.W. Rhim, Preparation of nanocellulose from micro-crystalline cellulose: the effect on the performance and properties of agar-based composite films, Carbohydr. Polym. 135 (2016) 18–26, https://doi.org/10.1016/j.carbpol.2015.08.082.

[61] T.Í.S. Oliveira, M.F. Rosa, M.J. Ridout, K. Cross, E.S. Brito, L.M.A. Silva, S.E. Mazzetto, K.W. Waldron, H.M.C. Azeredo, Bionanocomposite films based on polysaccharides from banana peels, Int. J. Biol. Macromol. 101 (2017) 1–8, https://doi.org/10.1016/j.ijbiomac.2017.03.068.

[62] P. Balakrishnan, S. Gopi, M.S. Sreekala, S. Thomas, UV resistant transparent bionanocomposite films based on potato starch/cellulose for sustainable packaging, Starch/Staerke 70 (2018) 1–34, https://doi.org/10.1002/star.201700139.

[63] A.P.M. Silva, A.V. Oliveira, S.M.A. Pontes, A.L.S. Pereira, M. de sá M. Souza Filho, M.F. Rosa, H.M.C. Azeredo, Mango kernel starch films as affected by starch nanocrystals and cellulose nanocrystals, Carbohydr. Polym. 211 (2019) 209–216, https://doi.org/10.1016/j.carbpol.2019.02.013.

[64] V. Nessi, X. Falourd, J.-E. Maigret, K. Cahier, A. D'Orlando, N. Descamps, V. Gaucher, C. Chevigny, D. Lourdin, Cellulose nanocrystals-starch nanocomposites produced by extrusion: structure and behavior in physiological conditions, Carbohydr. Polym. 225 (2019), 115123. https://doi.org/10.1016/j.carbpol.2019.115123.

[65] D. Liu, Y. Dong, D. Bhattacharyya, G. Sui, Novel sandwiched structures in starch/cellulose nanowhiskers (CNWs) composite films, Compos. Commun. 4 (2017) 5–9, https://doi.org/10.1016/j.coco.2017.03.001.

[66] X. Cao, Y. Chen, P.R. Chang, A.D. Muir, G. Falk, Starch-based nanocomposites reinforced with flax cellulose nanocrystals, Express Polym Lett 2 (2008) 502–510, https://doi.org/10.3144/expresspolymlett.2008.60.

[67] M. Yadav, K. Behera, Y.H. Chang, F.C. Chiu, Cellulose nanocrystal reinforced chitosan based UV barrier composite films for sustainable packaging, Polymers (Basel) 12 (2020) 202, https://doi.org/10.3390/polym12010202.

[68] R. Talja, Preparation and Characterization of Potato Starch Films Plasticized With Polyols, http://scholar.google.com/scholar?hl=en&btnG=Search&q=intitle:Preparation+and+characterization+of+potato+starch+films+plasticized+with+polyols#0 2007.